Real-Time Structural Investigation of a Lipid Bilayer during Its Interaction with Melittin Using Sum Frequency Generation Vibrational Spectroscopy

Xiaoyun Chen, Jie Wang, Cornelius B. Kristalyn, and Zhan Chen
Department of Chemistry, University of Michigan, Ann Arbor, Michigan 48109

ABSTRACT Interactions between membrane bilayers and peptides/proteins are ubiquitous throughout a cell. To determine the structure of membrane bilayers and the associated peptides/proteins, model systems such as supported lipid bilayers are often used. It has been difficult to directly investigate the interactions between a single membrane bilayer and peptides/proteins without exogenous labeling. In this work we demonstrate that sum frequency generation vibrational spectroscopy can be employed to study the interactions between peptides/proteins and a single lipid bilayer in real time, in situ, and without exogenous labeling. Using melittin and a dipalmitoyl phosphatidylglycerol bilayer as a model system, we monitored the C-H and C-D stretching signals from isotopically symmetric or asymmetric dipalmitoyl phosphatidylglycerol bilayers during their interaction with melittin. It has been found that the extent and kinetics of bilayer perturbation induced by melittin are very sensitive to melittin concentration. Such concentration dependence is correlated to melittin's mode of action. Melittin is found to function via the early and late stage of the carpet model at low and high concentrations, respectively, whereas the toroidal model is probable at intermediate concentrations. This research illustrates the potential of sum frequency generation as a biophysical technique to monitor individual leaflet structure of lipid bilayers in real time during their interactions with biomolecules.

INTRODUCTION

Interactions between a membrane bilayer and proteins/peptides are ubiquitous throughout a cell. Encoded by its sequence, every protein/peptide is designed to interact with membrane bilayers in a specific manner. For example, cytosolic proteins interact very weakly with, or even repel, the bilayer whereas peripheral or integral membrane proteins associate tightly with lipid bilayers (1,2). There are also peptides such as antimicrobial peptides (AMPs) that are designed to interact so strongly with certain types of membrane bilayers that they can disrupt the bilayers and disable their barrier function (3,4). Besides naturally occurring biomolecules, an increasing number of drug molecules are designed to target receptors on cell membranes or membranes themselves (or at least need to be transported across a membrane bilayer) (5,6). It is of fundamental importance to gain a molecular understanding of how membrane lipid bilayers behave during such interactions.

One intrinsic difficulty involved in studying such interactions is the extreme sensitivity required for a biophysical/analytical technique to follow the interactions at a molecular level in real time. Biochemical properties of peptides/proteins (e.g., adsorption/desorption coefficients, secondary structures, etc.) and lipid bilayers (e.g., hydrophobic tail orientation, phase information, etc.) can be obtained in carefully designed bulk experiments using liposomes or bicelles. Signals from biomolecules in solution may dominate over the interfacial signals of interest in such studies. Aligned multibilayers can solve these issues, but a possible drawback for aligned multibilayers is that peptides/proteins can access bilayers from both sides, whereas for real cells these peptides/proteins usually have access to only one side of a bilayer (e.g., the extracellular side or cytoplasmic side). There are several surface-sensitive techniques that can be employed in monitoring biomolecule adsorption onto a lipid bilayer, such as quartz crystal microbalance, calorimetry, surface plasmon resonance (SPR), etc. However, little structural insight can be directly obtained from these techniques. Additionally, few structure-determination techniques provide lipid-biomolecule interaction kinetics information. Recently, sum frequency generation (SFG) has been demonstrated to be a powerful tool to investigate structure and orientation of various biomolecules such as lipids (7–14) and proteins (15–27). In this study we will demonstrate that interactions between a bilayer and biomolecules can be monitored by SFG without any exogenous labeling in real time in situ. SFG can offer novel and complementary information because the signals involved are vibrational spectra, which are determined by the fundamental molecular structure of interfacial species. In addition SFG, as a second-order nonlinear laser spectroscopy technique, is intrinsically surface sensitive and can single out chemical and structural information from only the interfacial molecules against the overwhelming bulk contribution (28). The interactions between a single lipid bilayer and bee venom peptide melittin will be investigated as an example.

Melittin is among the best studied membrane-active peptides (29–32). It is composed of 26 amino acid residues. The first 20 residues in the N-terminus are mostly neutral and hydrophobic, with only one charged lysine at position seven, whereas the C-terminus is highly charged, with two lysine residues, two arginine residues, and the C-terminus amidated. Crystal structure of melittin has been solved (32,33).

Submitted October 18, 2006, and accepted for publication April 3, 2007.

Address reprint requests to Zhan Chen, Fax: 734-647-4685; E-mail: zhanc@umich.edu.

Editor: Lukas K. Tamm.

0006-3495/07/08/866/10 $2.00

doi: 10.1529/biophysj.106.099739

NMR structures of melittin reconstituted in various environments have also been obtained (34–37). In addition, other biophysical techniques such as neutron reflection (38), circular dichroism (39), fluorescence spectroscopy (40), attenuated total reflectance-Fourier transform infrared spectroscopy (ATR-FTIR) (41), and second harmonic generation (42), etc. have been applied to study the interactions between melittin and lipid bilayers. Melittin adopts a disordered structure in aqueous solution with low ion strength and converts to an α-helical structure upon association with lipid bilayers. Due to the proline 15 residue, the helix has a kink in the middle and the bend angle caused by this kink has been found to be dependent on the environment (35,36). As with many other cationic AMPs, it is generally believed that melittin can destabilize cell membranes by associating with membrane lipid bilayers and form membrane-peptide complexes after a threshold surface concentration of melittin is reached. However as is the case for many other cationic AMPs, the exact mode of action (e.g., how peptides associate with lipids and what complex structures they form) for melittin remains controversial (3,4). Different models have been proposed such as carpet-like, detergent-like, and formation of toroidal or barrel-stave pores inside the bilayer matrix, with research results supporting each of them (38,43–47).

The SFG technique has been extensively discussed (48–56). A series of recent publications from the Conboy group and several other groups demonstrates the advantages of SFG for lipid-bilayer studies (7–12). SFG allows the label-free determination of lipid flip-flop rate; and the results that phosphatidylcholines with dimyristoyl or dipalmitoyl acyl chains flip-flop rapidly under room temperature and body temperature attest to the molecular insights obtainable from this new technique. A brief introduction is given in the Supplementary Material about how SFG signals from the methyl groups can be related to their orientation, because bilayer structural perturbation deduced based on methyl symmetric stretching intensity will be extensively utilized in our analysis. An understanding of how the lipid acyl chain terminal methyl symmetric stretching mode intensity is modulated by the methyl group number density, molecular orientation, and orientation distribution is vital in the interpretation and understanding of many of the results presented below.

MATERIALS AND METHODS

Melittin was purchased from Sigma-Aldrich (St. Louis, MO), with a minimum concentration of 85% and a phospholipase A_2 activity <5 units/mg. Hydrogenated and deuterated 1,2-dipalmitoyl(D62)-*sn*-glycero-3-phosphoglycerol (DPPG and dDPPG) were purchased from Avanti Polar Lipids (Alabaster, AL). DPPG bilayers were used in this research because it is an important lipid component for bacterial cell membrane but exists in negligible quantity in most mammalian cell membranes. The negative charges on DPPG bilayers would ensure strong interactions with melittin. Right-angle fused silica prisms and CaF_2 prisms were purchased from Altos (Trabuco Canyon, CA). Both types of prisms were soaked in toluene overnight and then sonicated in Contrex AP solution from Decon Labs (King of Prussia, PA) before the first usage. Before each deposition, fused silica prisms were soaked in heated potassium dichromate/sulfuric acid solution for an hour. CaF_2 prisms were soaked in Contrex AP solution overnight and then rinsed with water before soaking in methanol for an hour. Both types of prisms were rinsed thoroughly with an ample amount of deionized water and then cleaned inside a glow charge plasma chamber for ~4 min immediately before bilayer preparation. Substrates were tested using SFG, and no contamination was detected.

We used the Langmuir-Blodgett and Langmuir-Schaefer (LB/LS) methods to deposit the proximal and the distal leaflets, respectively (9,57,58). A KSV2000 LB system and ultrapure water from a Millipore system (Millipore, Bedford, MA) were used throughout the experiment for bilayer preparation. Briefly, a prism was attached to a sample holder via one right-angle face so that the other right-angle face was perpendicularly immersed in the water inside the Langmuir trough. An appropriate amount of lipid chloroform solution was then gently spread onto the water surface, and the chloroform was allowed to evaporate. The monolayer area was compressed by two barriers at a rate of 5 mm/min until a surface pressure of 34 mN/m was reached. The prism was lifted out of the subphase at a rate of 2 mm/min. Before depositing the distal leaflet, a 1.8-mL reservoir was placed in a large trough slightly deeper than it so that water could cover it as shown in Fig. S2 (Supplementary Material). A monolayer of lipid at 34 mN/m surface pressure was prepared, onto which the prism's monolayer-coated right-angle face was horizontally lowered. After the formation of the bilayer, the extra lipids at the air-water interface were sucked away. Water in the large trough was drained while keeping the bilayer immersed in water inside the small reservoir so that a much smaller amount of peptide/protein could be sufficient for the experiment. The bilayer was immersed in water throughout the entire experiment, and a small amount of water could be added to the reservoir to compensate for evaporation when needed for long timescale experiments. For melittin-bilayer interaction experiments, ~100 μL melittin solution of appropriate concentration was injected into the reservoir to achieve the desired concentration. A magnetic microstirrer was used to ensure a homogeneous concentration distribution of peptide molecules in the subphase below the bilayer. All experiments were carried out at room temperature (24°C), at which a DPPG bilayer should be in the gel phase.

Details of the SFG setup in our lab have been described in previous publications and will not be repeated here (53,54). Input laser beams were incident onto one of the right-angle faces of a prism and then reflected by the other right-angle face coated with the bilayer, as shown in Fig. S2. The prism was arranged so that the total reflection for the 532-nm green beam was just achieved. Under this condition, the infrared (IR) beam was not total reflected.

RESULTS

Examination of molecular structures of supported lipid bilayers on SiO_2 and CaF_2

A variety of substrates have previously been used as solid supports for lipid bilayers, with mica and silica being the most frequently used (57–59). To allow the study of amide I (1600 cm^{-1} ~1700 cm^{-1}) and C-D (2000 cm^{-1} ~2250 cm^{-1}) stretching modes, we explore the application of CaF_2 as the substrate material due to its broader IR transmission range.

Four types of supported lipid bilayers were prepared on SiO_2 and CaF_2 substrates: dDPPG/DPPG (dDPPG as the proximal leaflet and DPPG as the distal leaflet), DPPG/dDPPG, dDPPG/dDPPG, and DPPG/DPPG. SFG spectra in the C-H stretching range of these selectively deuterated bilayers are displayed in Fig. 1. Spectra for isotopically asymmetric bilayers on both substrates are dominated by

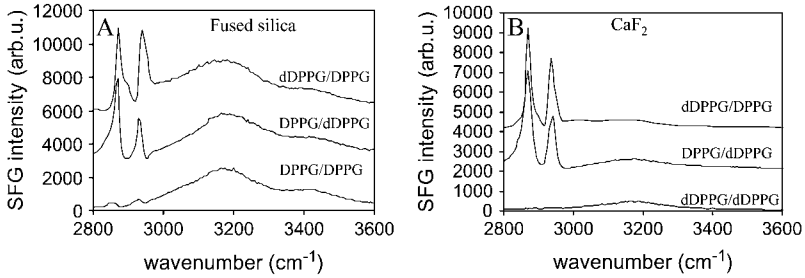

FIGURE 1 SFG spectra from DPPG bilayers with selectively deuterated leaflets constructed on fused silica (*A*) and CaF_2 (*B*) prism substrates. Neighboring spectra are offset for clarity for all figures.

CH_3 symmetric stretching mode (~2875 cm^{-1}) and Fermi resonance (~2940 cm^{-1}). The broad peaks centered around 3180 cm^{-1} and 3400 cm^{-1} originate from the O-H stretching modes of interfacial water molecules that were aligned by the surface charges. The strong C-H signals from dDPPG/DPPG bilayers and DPPG/dDPPG bilayers on both substrates indicate that stable and ordered bilayers formed on both substrates. Weak C-H signals from isotopically symmetric bilayers on both substrates indicate that the proximal leaflet and distal leaflet had very similar structures and signals generated from them effectively cancelled each other. From the above observation, it can be concluded that DPPG bilayers in the gel phase can be successfully prepared using the LB/LS method. The different spectral features between corresponding spectra in Fig. 1, *A* and *B*, can be attributed to the different O-H signals and the different interference patterns they caused, as SiO_2 surfaces were more negatively charged than CaF_2 surfaces under our experimental conditions and therefore induced better ordering in interfacial water molecules (60).

With the use of the CaF_2 prism, the C-D stretching range can now be probed to obtain structural information of the deuterated leaflet. Shown in Fig. 2 is the C-D stretching spectrum of a dDPPG/DPPG bilayer on a CaF_2 substrate.

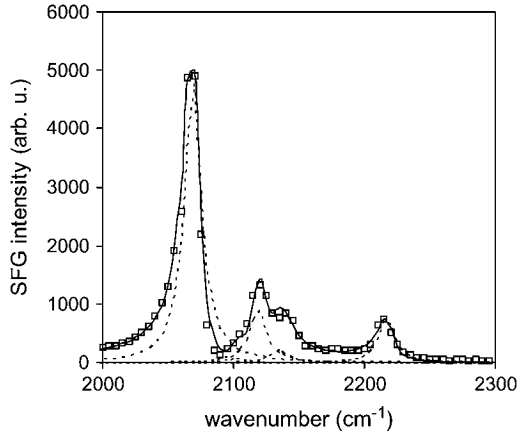

FIGURE 2 SFG spectra collected from a dDPPG/DPPG bilayer on CaF_2 in the C-D stretching range and the spectral fitting results. Square: experimental data; solid line: overall fitting results; dotted line: component peaks used in fitting. Spectral fitting was performed using Eq. S4 in the Supplementary Material. A nonresonant background of 2 was used in fitting.

The dominant peak at 2070 cm^{-1} can be attributed to CD_3 symmetric stretching mode. Without the strong interference from O-H bands, the C-D spectra of dDPPG/DPPG and DPPG/dDPPG are very similar, and therefore the C-D spectrum for the later is not shown here. Strong SFG C-D signals indicate an ordered dDPPG leaflet, further confirming the existence of an ordered bilayer. Traditionally, fluorescence microscopy and fluorescence recovery after photobleaching have been employed to verify the quality of supported bilayers. They offer important information regarding the fluidity, domain structure, and integrity of a bilayer. However they provide little insight regarding the molecular organization within the bilayer. SFG is an ideal technique to provide such complementary information.

Another advantage of choosing CaF_2 as the substrate is its relatively neutral surface around pH 7. The negative surface charges of other conventional solid support materials such as SiO_2 and mica surfaces may cause artifacts in experiments, as it has been reported that the substrate charge can affect charged molecule distribution in model lipid bilayers (59,61). Melittin is highly positively charged around pH 7, and thus the electrostatic interactions between melittin and a negatively charged substrate can be exceptionally strong, necessitating the usage of a relatively neutral substrate such as CaF_2.

Investigation of melittin-bilayer interactions using isotopically symmetric or asymmetric bilayers

Typically the C-D and C-H stretching signals from a dDPPG/DPPG or DPPG/dDPPG bilayer remain stable over more than 10 h (results not shown), allowing the study of structural changes of each leaflet of a bilayer induced by melittin adsorption within this time window. We have employed two strategies in studying the bilayer structural changes induced by melittin. For the first strategy, an isotopically symmetric bilayer (e.g., DPPG/DPPG) is employed and a symmetry breaking of the bilayer caused by melittin is indicated by an increase in lipid acyl chain terminal methyl symmetric stretching SFG signals. Such signals shed light on how differently the two leaflets of a bilayer are perturbed by melittin. The second strategy is to use an isotopically asymmetric bilayer (e.g., dDPPG/DPPG), allowing us to study how each individual leaflet interacts with melittin

using signals in C-H and C-D stretching ranges. A small amount of phospholipase present in the melittin sample was found to induce changes in gold-supported 1-palmitoyl-2-oleoyl-*sn*-glycero-3-phosphocholine (POPC) bilayers previously (46). However phospholipase's effect was found to be negligible in our experiment, as almost identical results were observed from experiments using or without using EDTA and from experiments using synthetic melittin (Axxora Life Science, San Diego, CA).

According to the first strategy, an isotopically symmetric dDPPG/dDPPG bilayer was prepared. A dDPPG/dDPPG bilayer instead of a DPPG/DPPG bilayer was used to avoid possible SFG C-H stretching signal confusion from melittin. Spectra of a dDPPG/dDPPG bilayer on CaF_2 before and after interacting with 0.78 μM melittin solution are shown in Fig. 3 *A* (C-D stretching range) and Fig. 3 *B* (C-H stretching range). Before the injection of melittin, only weak SFG signals were observed from the bilayer due to the signal cancellation as discussed above. After the injection of melittin, SFG C-D stretching signals started to appear; the final spectrum is shown in Fig. 3 *A*. Comparing the spectrum in the C-D stretching region after interacting with melittin to that of a dDPPG/DPPG bilayer as shown in Fig. 2, we observed very similar spectral features. This indicates that melittin caused the distal leaflet dDPPG to generate weaker signals that could no longer cancel the C-D signals from the proximal leaflet. The signals in the C-H/O-H stretching region also underwent remarkable changes as shown in Fig. 3 *B*. The O-H stretching peak centered around 3180 cm^{-1} almost vanished completely due to charge neutralization by melittin, whereas a new feature centered around 3290 cm^{-1} is observed, which could be attributed to the amide A mode of melittin or the N-H stretching mode of side chains such as those in lysine and arginine (62). Relatively weak features around 2870 cm^{-1} could also be observed, which might originate from the symmetric stretching mode of methyl containing residues of melittin, such as leucine and alanine, or the undeuterated glycerol and headgroup moieties in dDPPG.

A similar study was carried out using a dDPPG/DPPG bilayer according to the second strategy. Shown in Fig. 4 are spectra of a dDPPG/DPPG bilayer on CaF_2 before and after interacting with 0.78 μM melittin solution. In the C-D stretching range, there was a large signal intensity decrease (~10-fold) for the 2070 cm^{-1} peak from CD_3 symmetric stretching mode (Fig. 4 *A*). The spectral features remained similar, with a slightly larger contribution from deuterated methylene vibrational modes around 2100 cm^{-1} (CD_2 symmetric stretching) and 2200 cm^{-1} (CD_2 asymmetric stretching). This is in accordance with the previous observation that disordering in acyl chain should lead to more *gauche* conformation (8,13,63).

The C-H/O-H stretching spectrum underwent more substantial changes (Fig. 4 *B*). The C-H signal intensity decreased more than 300-fold, indicative of an extensive ordering or orientational change of distal DPPG acyl chain terminal methyl groups caused by melittin. As we learned in using the dDPPG/dDPPG system above, melittin and dDPPG may also contribute C-H signals and thus the final weak C-H stretching signals may be partially a result of interference. By using a DPPG/dDPPG bilayer (instead of a dDPPG/DPPG bilayer as discussed here), a thorough disturbance of the distal leaflet was also observed (results not shown). Similar to what was observed for the dDPPG/dDPPG experiment shown above, the O-H signals also decreased, whereas N-H signals (~3280 cm^{-1}) increased.

Assuming that a dDPPG/dDPPG bilayer and a dDPPG/DPPG bilayer interact with melittin in the same manner, it is puzzling to observe that the spectral intensity at 2070 cm^{-1} after bilayer-melittin interactions was larger for the dDPPG/dDPPG bilayer (intensity ~1350) than the dDPPG/DPPG bilayer (intensity ~480). The proximal dDPPG leaflets from both systems should be disturbed to the same extent by melittin. The C-D symmetric stretching signal from the former system could be partially cancelled by the distal dDPPG leaflet, whereas the latter system's distal DPPG leaflet would not cancel out any C-D signals. Therefore the dDPPG/DPPG bilayer should always give a stronger CD_3 2070 cm^{-1} peak than the dDPPG/dDPPG bilayer, contrary to what we observed in Figs. 3 *A* and 4 *A*. This puzzling observation can only be explained if we consider the transmembrane movement, or flip-flop, of lipids (64). If there had been a complete transmembrane mixing of lipids, the signal generating CD_3 groups in the proximal leaflet should have half the number density in a dDPPG/DPPG bilayer compared to that in a dDPPG/dDPPG bilayer. This difference in number density in turn should lead to a fourfold intensity difference. The observed intensity difference is ~3-fold, suggesting either

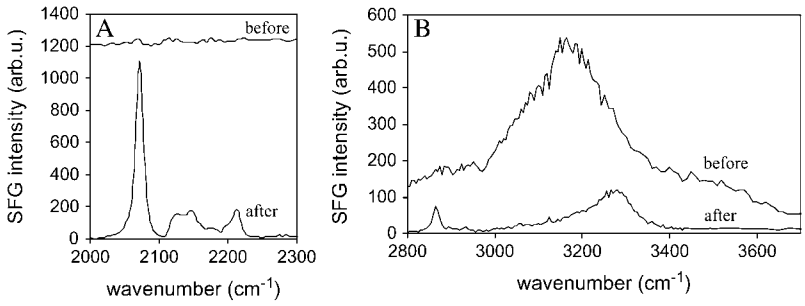

FIGURE 3 Structural perturbation of a dDPPG/dDPPG bilayer on CaF_2 induced by melittin at a solution concentration of 0.78 μM. (*A*) SFG spectra in the C-D stretching range before and after interacting with melittin; (*B*) C-H/O-H stretching signals before and after interacting with melittin.

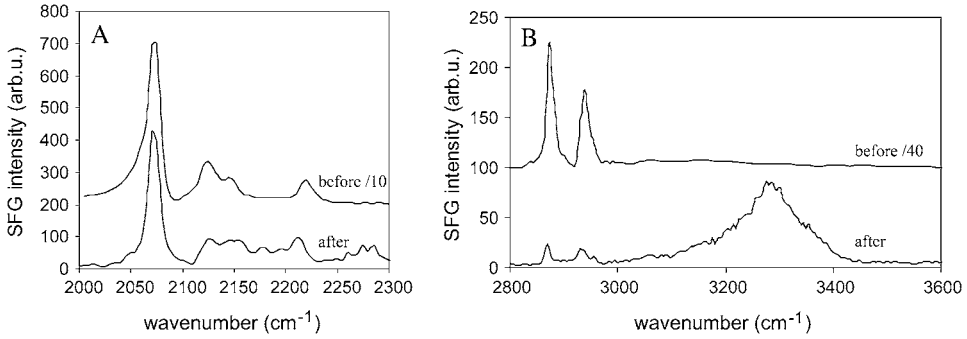

FIGURE 4 Structural perturbation of a dDPPG/DPPG bilayer on CaF_2 induced by melittin at a solution concentration of 0.78 μM. (*A*) SFG spectra in the C-D stretching range before and after interacting with melittin; (*B*) C-H/O-H stretching signals before and after interacting with melittin.

an incomplete transmembrane mixing or interference from the C-D signals contributed by the significantly perturbed distal leaflet. A more quantitative analysis can be found in the discussion and in the Supplementary Materials.

Concentration dependence of melittin-bilayer interactions

In previous antibacterial assays, melittin was found to have a minimum inhibitory concentration (MIC) in the range of 0.2–16 μM for various bacteria (65–67). Solution concentrations encompassing this range were studied in our research, and Fig. 5 shows the SFG spectra for dDPPG/DPPG bilayers after they interacted with melittin solution at three representative concentrations.

At 0.156 μM (top spectra in Fig. 5, *A* and *B*), signals from both the distal and proximal leaflets were clearly discernible and resembled that of the original unperturbed bilayer, though the distal C-H signal diminished to a greater extent. Some shoulder peaks also manifested themselves in the top spectrum in Fig. 5 *B*, indicating disordering in the bilayer. As discussed in the previous section, the bilayer experienced more extensive perturbation at 0.78 μM. However the proximal leaflet retained much of its ordered structure, as significant signals in the C-D stretching range were observable even after the signal weakening caused by flip-flop (the middle spectrum in Fig. 5 *A*).

At 6.25 μM (bottom spectra in Fig. 5), C-H signals from the distal leaflet no longer resembled the original unperturbed bilayer spectral features. Due to spectral interference between lipid C-H and melittin C-H stretching signals, which was not negligibly weak at solution concentrations as low as 0.78 μM (as can be seen in Fig. 3), we will not attempt to further analyze the C-H stretching region results—though it is feasible to analyze them after careful spectral fitting and deconvolution. Unlike C-H spectra, C-D spectral features always remained more or less discernible, indicating a less extensive perturbation. ATR-FTIR results indicate that there was significant lipid displacement at this concentration (results not shown). Therefore we believe that the melittin-induced signal decrease for asymmetric bilayers can be due to multiple reasons, including a loss of asymmetry caused by transmembrane mixing of hydrogenated and deuterated lipids and structural perturbation of the lipids (both orientation and ordering), displacement of lipids by melittin, and spectral interference for signals in the C-H stretching range. More details regarding the exact causes of melittin-induced bilayer signal decrease will be discussed further in the Discussion section.

Real-time monitoring of bilayer perturbation induced by melittin

Time-dependent SFG studies have been applied to investigate kinetics regarding surfaces and interfaces including bilayers (12,68). In Fig. 6 the CD_3 symmetric stretching peak intensity from a dDPPG/dDPPG bilayer on a CaF_2 prism is monitored at 2070 cm^{-1} as a function of time after injecting melittin at time 0 s. Before the injection of melittin, the symmetric dDPPG/dDPPG bilayer generated almost no CD_3 symmetric stretching signals. At high solution concentrations between 7.8 μM and 1.56 μM, the peak intensity reached maximum immediately after the injection of melittin and then decreased. The lower the concentration, the stronger

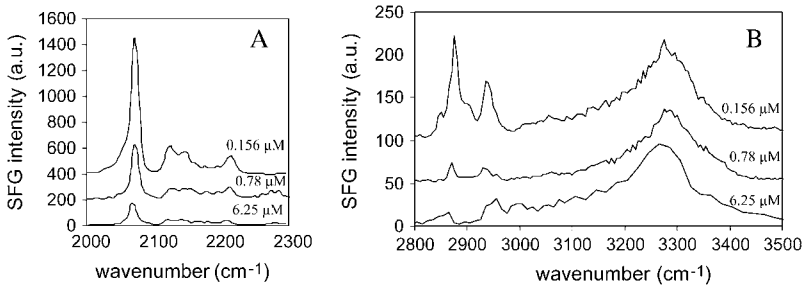

FIGURE 5 Structural perturbation of a dDPPG/DPPG bilayer on CaF_2 induced by three melittin solution concentrations in the (*A*) C-D stretching range and the (*B*) C-H/O-H stretching range.

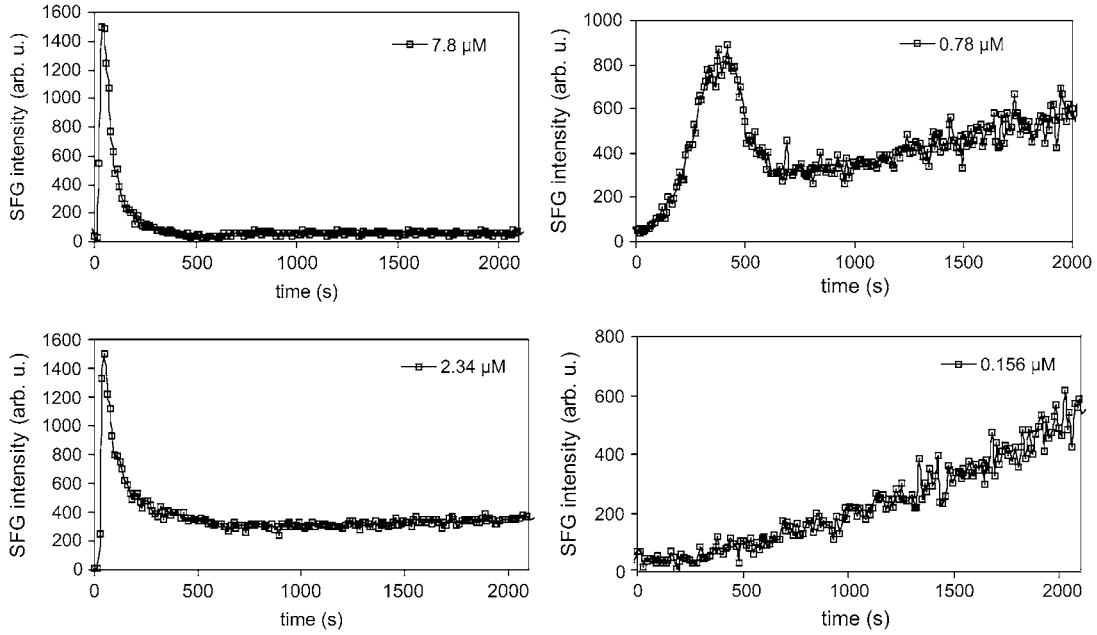

FIGURE 6 Signal intensity change at 2070 cm^{-1} monitoring melittin interacting with dDPPG/dDPPG bilayers on CaF_2. Melittin stock solution was injected into the subphase at time 0 s. Four solution concentrations were used, and dramatically different patterns were observed.

the final CD_3 symmetric stretching signals. For melittin concentrations at 0.78 μM, the CD_3 peak intensity underwent a gradual increase after the initial increase/decrease pattern. For concentrations even lower (e.g., 0.156 μM), the initial intensity increase process took a much longer time to complete.

Experiments to follow such time-dependent spectral intensity change were also performed for asymmetric bilayers; representative results are shown in Fig. 7 for dDPPG/DPPG bilayers interacting with melittin solutions of various concentrations. The CD_3 and CH_3 symmetric stretching modes from the proximal and the distal leaflets were simultaneously monitored at 2070 cm^{-1} and 2875 cm^{-1}. It should be noted that the 2875 cm^{-1} peak intensity in Fig. 7 was normalized to that of the 2070 cm^{-1} peak, so that CD_3 and CH_3 symmetric stretching modes have the same initial signal intensities before melittin-induced signal changes. Such normalization

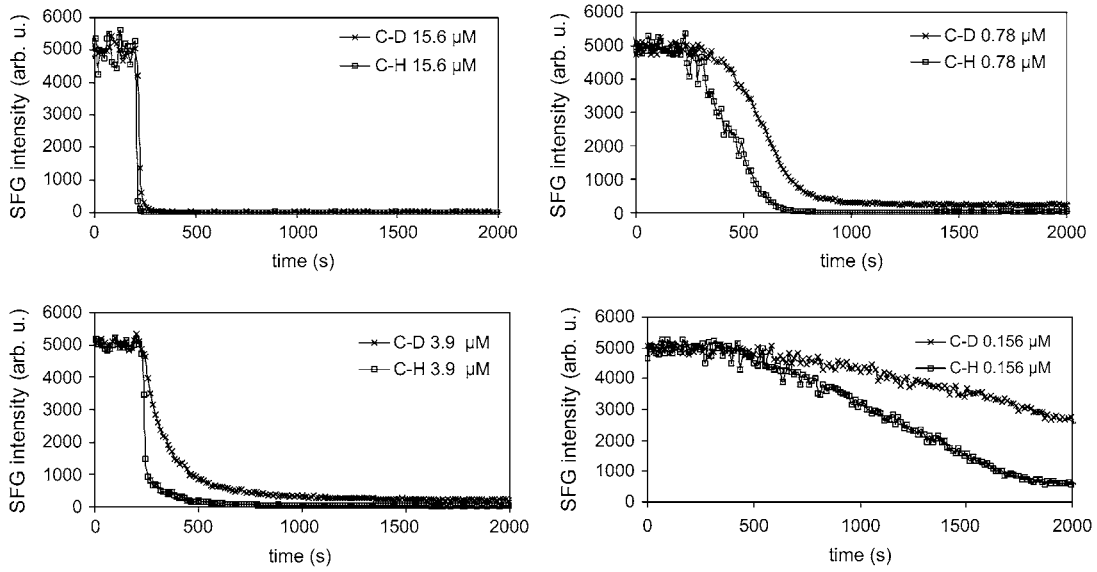

FIGURE 7 Signal intensity change at 2070 cm^{-1} and 2875 cm^{-1} monitoring melittin interacting with dDPPG/DPPG bilayers on CaF_2. Melittin stock solution was injected into the subphase at 200 s. Four solution concentrations were used, and dramatically different patterns were observed.

simplifies not only the interpretation of Fig. 7 but also the later quantitative analysis. Strong and stable signals from both leaflets were observed before melittin injection at 200 s. Similar to the trend observed in Fig. 6, in Fig. 7 the spectral changes occurred very quickly and then signals became stable at higher concentrations, whereas a much longer time was required for the intensity to become stable for lower melittin concentrations. Very weak final signals from both leaflets were observed after the peptide-lipid interactions when 0.78 μM or higher melittin solution concentrations were used. At a solution concentration of 0.156 μM or lower, strong SFG signals from the proximal dDPPG leaflet could still be observed after a prolonged period of time.

DISCUSSION

Concentration-dependent mode of action

AMPs are designed by nature for the host organisms to fend off the invasion of exogenous pathogens as the first immune reaction before other slower responses such as adaptive immune response take place. A sufficient local concentration is critical in determining whether the peptides can kill the invading species. Though not an AMP by definition, melittin has been shown to have a threshold surface concentration beyond which the association state between melittin and bilayers can undergo a fundamental change from the surface-associated state to an inserted state (38,43). However many previous studies were carried out with multilayers of lipids, which may not reflect the true mode of interactions between melittin and a single bilayer membrane.

Both the rate and the mode of melittin-bilayer interactions are clearly concentration dependent (Figs. 5–7 and S3). At high solution concentrations (>3 μM), both leaflets were significantly disrupted by melittin within minutes, as shown in Fig. 6 (7.8 μM and 2.34 μM) and Fig. 7 (15.6 μM and 3.9 μM). In addition to bilayer structure perturbation and flip-flop, ATR-FTIR results (Fig. S3) indicated that lipid displacement from the substrate surface also contributed to the signal decrease. At intermediate concentrations (between 0.5 μM and 3 μM), relatively weak signals were observed from the dDPPG/DPPG system (Fig. 7 0.78 μM), but significant signals were observed from the dDPPG/dDPPG system (Fig. 6 2.34 μM and 0.78 μM). As only negligible lipid displacement was observed at these concentrations, such signal changes resulted purely from bilayer structural perturbation and flip-flop. The relatively strong signals observed from the dDPPG/dDPPG system indicated that there was a large structural asymmetry between the two leaflets. This led us to conclude that whereas the distal leaflet was extensively perturbed, the proximal leaflet only suffered limited perturbation at these concentrations. To further distinguish the contribution of structural perturbation and flip-flop, a more quantitative analysis based on Figs. 6 and 7 was carried out; the details can be found in the Supplementary Material. According to the analysis developed therein, it could be concluded that significant flip-flop occurred at the intermediate concentrations, as the intensity of the 2070 cm^{-1} peak of the dDPPG/DPPG bilayer was weaker than that of the dDPPG/dDPPG bilayer ~500~1000 s after the injection of melittin (comparing 0.78 μM kinetics curves in Figs. 6 and 7). At low solution concentrations of melittin (<0.5 μM), interactions between melittin and a DPPG bilayer proceeded slowly, requiring hours before reaching an equilibrium. During this process, the distal leaflet underwent more substantial structural perturbation compared to the proximal leaflet, but no significant lipid flip-flop occurred at these concentrations, as the intensity of the 2070 cm^{-1} peak of the dDPPG/DPPG bilayer remained stronger than that of the dDPPG/dDPPG bilayer. As it is unlikely to maintain the certain concentration of peptides under physiological conditions without their being digested or metabolized, longer timescale results are not discussed here.

Equipped with the above details of melittin-bilayer interactions at a broad concentration range, we can attempt to clarify the mode of interactions between melittin and cell membranes and to correlate it to previous biological assay results. At low melittin solution concentrations (<0.5 μM), only the distal leaflet is significantly perturbed, corresponding to the surface-associated state or the early stage of the carpet model (4,44). Such a perturbation in the distal leaflet alone is unlikely to cause fatal damage to a cell, when the proximal leaflet retains its structural integrity. This phenomenon was previously observed with SFG for a small antibiotic oligomer (69). As only the distal leaflet is affected, the hydrophobic interior of the bilayer is conserved and therefore no significant transmembrane flip-flop motion of lipids is observed. For intermediate melittin concentrations (between 0.5 μM and 3 μM), the distal leaflet is more thoroughly perturbed; however the proximal leaflet remains more or less undisrupted. Significant transmembrane movement of lipids is observed to occur within this concentration range. The enhanced rate of lipid flip-flop is likely due to toroidal pores formed by a fraction of the adsorbed melittin molecules, as such pores are capable of facilitating the transmembrane movement of lipids via the hydrophilic pore while still maintaining an undisrupted bilayer (64). In a recent publication from our group studying the same system, the orientation of interfacial melittin molecules when interacting with a DPPG/DPPG bilayer was deduced based on the melittin amide I signals at a solution concentration of 0.78 μM (70). It was found that about three-quarters of melittin molecules orient parallel to the bilayer surface, whereas the rest orient more or less perpendicularly inside a bilayer. This agrees with the C-H/C-D stretching results presented above: the parallel fraction causing the disruption of the distal leaflet and the perpendicular fraction facilitating the transmembrane flip-flop. For even higher concentrations (>3 μM), significant lipid displacement was observed, indicating that melittin is functioning as a detergent solubilizing the lipids, corresponding to the late stage of the carpet model (44).

It is likely that for different types of cells, the critical concentration may correspond to different molecular events. For cells whose membrane asymmetry is vital for their survival, the critical concentration should be defined with regard to the onset of transmembrane mixing of the two leaflets. In contrast, such a critical concentration may bear little biological meaning for cells whose survival only depends on the integrity of the cytoplasmic leaflet. Instead it would be more appropriate to define the MIC for such cells as the concentration beyond which lipid displacement occurs or at which the proximal (cytoplasmic) leaflet suffers significant disruption. It is encouraging to note that the critical concentration ranges (significant disruption for both leaflets at $\sim$3 μM and significant transmembrane mixing at $\sim$0.5 μM) extracted from our results are within the MIC ranges (0.2–16 μM) obtained through various bacterium-based assays (65–67). The small deviation is likely a combined result of the model bilayer composition and phase. The DPPG (or dDPPG) monolayer at 34 mN/m was used in preparing the bilayer so that the dDPPG/DPPG bilayer could maintain the isotopic asymmetry in the gel phase. Therefore care should be taken in comparing results obtained from such model systems to cell-based studies.

Sequence of events

Peptide/protein adsorption onto a lipid bilayer can be viewed as proceeding via several consecutive steps: partitioning into the vicinity of a bilayer, converting from its solution structure to a membrane-associated structure, and insertion into and association within the bilayer (71,72). However, to experimentally observe these processes taking place directly in real time is challenging. Fluorescence from Trp^{19} of melittin has recently been employed to study the insertion kinetics of melittin (40). Here we show that SFG time-dependent C-H and C-D stretching signals can provide complementary information about the bilayer response during the interaction process.

Several interesting details regarding bilayer-melittin interactions can be learned from our SFG results. Figs. 6 and 7 show that melittin can effectively disturb the distal leaflet first (corresponding to the extracellular side of a membrane bilayer for cells), and during this period the proximal leaflet (corresponding to the cytoplasmic side of a membrane bilayer for cells) can still remain more or less unperturbed. Spectral intensity changes were also monitored for other vibrational modes such as the water O-H stretching mode around 3180 cm^{-1} and melittin amide I mode around 1655 cm^{-1} (results not shown here). The former is sensitive to the surface electric field, whereas the latter is sensitive to melittin adsorption orientation and amount. It was observed that spectral intensity from all these modes occurred almost concomitantly, with the O-H stretching signal decreased slightly before the change in amide I and bilayer signals.

Taken together, our results show that melittin molecules partition into the vicinity of the DPPG bilayer surface as the first step, as the O-H signal decreased first. This is probably driven by the electrostatic attractions between melittin and negatively charged DPPG. Adsorption of melittin onto the bilayer occurs simultaneously as melittin starts to interact with the distal leaflet that melittin molecules directly contact, as the amide I and bilayer signals changed simultaneously. After that, the proximal leaflet also starts to interact with melittin molecules, either by direct perturbation of melittin or by forming a certain type of complex such as pores or aggregates. The rates at which these steps take place are modulated by the surface concentration of melittin, which is in turn determined by the solution concentration of melittin. Similar sequences of events have previously been observed based on fluorescence and circular dichroism results, though all these steps were observed to take place within a few seconds after mixing melittin solution with vesicle solution (40). This discrepancy—partially due to the much higher concentration of melittin and the different experimental setup—may also be due to a hysteretic or delayed response of bilayer—as signals from bilayers instead of melittin were monitored here—demonstrating the importance of interrogating a system with different techniques.

In conclusion, SFG has the potential to provide novel information in the investigation of peptide/protein-membrane bilayer interactions. Such information includes the real-time structural perturbation experienced by both leaflets of a single lipid bilayer, adsorption kinetics, and orientation of a peptide/protein, water alignment, and surface charge state, etc. Taken together, such results can shed light on the molecular mode of interactions between cell membranes and other biomolecules. Here we have shown that the mode of interaction between melittin and a DPPG bilayer is highly dependent on the melittin solution concentration. The well-defined supported bilayer system makes it easy to correlate such findings to the results obtained using other biophysical techniques or from computer simulations (73).

In addition to the interactions between bilayers and AMPs, SFG can be applied to investigate many other intriguing biological events involving the interplay of peptides/proteins and a membrane bilayer. For example, SFG can also be employed to study the protein-induced membrane deformation (74), viral fusion proteins' mode of action and membrane fusion/fission mechanism in general (75–77), and membrane bilayer-cytoskeleton protein interactions (78), etc. With the development of polymer-cushioned supported bilayer or use of freestanding lipid bilayers, the substrate's influence can be greatly reduced (79). We believe that the sensitivity of SFG will make the supported bilayer system into a more informative model for cell membranes.

SUPPLEMENTARY MATERIAL

To view all of the supplemental files associated with this article, visit www.biophysj.org.

This work is supported by the Office of Naval Research (N00014-02-1-0832). X.C. thanks Eli Lilly for a bioanalytical fellowship.

REFERENCES

1. Lee, A. G. 2005. How lipids and proteins interact in a membrane: a molecular approach. *Mol. Biosyst.* 1:203–212.
2. McIntosh, T. J., and S. A. Simon. 2006. Roles of bilayer material properties in function and distribution of membrane proteins. *Annu. Rev. Biophys. Biomol. Struct.* 35:177–198.
3. Zasloff, M. 2002. Antimicrobial peptides of multicellular organisms. *Nature.* 415:389–395.
4. Brogden, K. A. 2005. Antimicrobial peptides: pore formers or metabolic inhibitors in bacteria? *Nat. Rev. Microbiol.* 3:238–250.
5. Cabiaux, V. 2004. pH-sensitive toxins: interactions with membrane bilayers and application to drug delivery. *Adv. Drug Deliv. Rev.* 56: 987–997.
6. Mouritsen, O. G., and K. Jorgensen. 1998. A new look at lipid-membrane structure in relation to drug research. *Pharm. Res.* 15:1507–1519.
7. Petralli-Mallow, T. P., K. A. Briggman, L. J. Richter, J. C. Stephenson, and A. L. Plant. 1999. Nonlinear optics as a detection scheme for biomimetic sensors: SFG spectroscopy of hybrid bilayer membrane formation. *Proc. SPIE.* 3858:25–31.
8. Doyle, A. W., J. Fick, M. Himmelhaus, W. Eck, I. Graziani, I. Prudovsky, M. Grunze, T. Maciag, and D. J. Neivandt. 2004. Protein deformation of lipid hybrid bilayer membranes studied by sum frequency generation vibrational spectroscopy. *Langmuir.* 20:8961–8965.
9. Liu, J., and J. C. Conboy. 2005. Structure of a gel phase lipid bilayer prepared by the Langmuir-Blodgett/Langmuir-Schaefer method characterized by sum-frequency vibrational spectroscopy. *Langmuir.* 21:9091–9097.
10. Liu, J., and J. C. Conboy. 2005. 1,2-diacyl-phosphatidylcholine flip-flop measured directly by sum-frequency vibrational spectroscopy. *Biophys. J.* 89:2522–2532.
11. Liu, J., and J. C. Conboy. 2004. Phase transition of a single lipid bilayer measured by sum-frequency vibrational spectroscopy. *J. Am. Chem. Soc.* 126:8894–8895.
12. Liu, J., and J. C. Conboy. 2004. Direct measurement of the transbilayer movement of phospholipids by sum-frequency vibrational spectroscopy. *J. Am. Chem. Soc.* 126:8376–8377.
13. Ohe, C., Y. Ida, S. Matsumoto, T. Sasaki, Y. Goto, A. Noi, T. Tsurumaru, and K. Itoh. 2004. Investigations of polymyxin B-phospholipid interactions by vibrational sum frequency generation spectroscopy. *J. Phys. Chem. B.* 108:18081–18087.
14. Ma, G., and H. C. Allen. 2006. DPPC Langmuir monolayer at the air-water interface: probing the tail and head groups by vibrational sum frequency generation spectroscopy. *Langmuir.* 22:5341–5349.
15. Kim, J., and G. A. Somorjai. 2003. Molecular packing of lysozyme, fibrinogen, and bovine serum albumin on hydrophilic and hydrophobic surfaces studied by infrared-visible sum frequency generation and fluorescence microscopy. *J. Am. Chem. Soc.* 125:3150–3158.
16. Mermut, O., D. C. Phillips, R. L. York, K. R. McCrea, R. S. Ward, and G. A. Somorjai. 2006. In situ adsorption studies of a 14-amino acid leucine-lysine peptide onto hydrophobic polystyrene and hydrophilic silica surfaces using quartz crystal microbalance, atomic force microscopy, and sum frequency generation vibrational spectroscopy. *J. Am. Chem. Soc.* 128:3598–3607.
17. Dreesen, L., C. Humbert, Y. Sartenaer, Y. Caudano, C. Volcke, A. A. Mani, A. Peremans, P. A. Thiry, S. Hanique, and J. M. Frere. 2004. Electronic and molecular properties of an adsorbed protein monolayer probed by two-color sum-frequency generation spectroscopy. *Langmuir.* 20:7201–7207.
18. Dreesen, L., Y. Sartenaer, C. Humbert, A. A. Mani, C. Methivier, C. M. Pradier, P. A. Thiry, and A. Peremans. 2004. Probing ligand-protein recognition with sum-frequency generation spectroscopy: the avidin-biocytin case. *Chemphyschem.* 5:1719–1725.
19. Wang, J., M. A. Even, X. Chen, A. H. Schmaier, J. H. Waite, and Z. Chen. 2003. Detection of amide I signals of interfacial proteins in situ using SFG. *J. Am. Chem. Soc.* 125:9914–9915.
20. Wang, J., M. L. Clarke, Y. B. Zhang, X. Chen, and Z. Chen. 2003. Using isotope-labeled proteins and sum frequency generation vibrational spectroscopy to study protein adsorption. *Langmuir.* 19:7862–7866.
21. Wang, J., S. M. Buck, and Z. Chen. 2003. The effect of surface coverage on conformation changes of bovine serum albumin molecules at the air-solution interface detected by sum frequency generation vibrational spectroscopy. *Analyst.* 128:773–778.
22. Wang, J., X. Chen, M. L. Clarke, and Z. Chen. 2005. Detection of chiral sum frequency generation vibrational spectra of proteins and peptides at interfaces in situ. *Proc. Natl. Acad. Sci. USA.* 102:4978–4983.
23. Wang, J., X. Chen, M. L. Clarke, and Z. Chen. 2006. Vibrational spectroscopic studies on fibrinogen adsorption at polystyrene/protein solution interfaces: hydrophobic side chain and secondary structure changes. *J. Phys. Chem. B.* 110:5017–5024.
24. Chen, X., J. Wang, J. J. Sniadecki, M. A. Even, and Z. Chen. 2005. Probing α-helical and β-sheet structures of peptides at solid/liquid interfaces with SFG. *Langmuir.* 21:2662–2664.
25. Clarke, M. L., J. Wang, and Z. Chen. 2005. Conformational changes of fibrinogen after adsorption. *J. Phys. Chem. B.* 109:22027–22035.
26. Chen, X., and Z. Chen. 2006. SFG studies on interactions between antimicrobial peptides and supported lipid bilayers. *Biochim. Biophys. Acta.* 1758:1257–1273.
27. Chen, X., M. L. Clarke, J. Wang, and Z. Chen. 2005. Sum frequency generation vibrational spectroscopy studies on molecular conformation and orientation of biological molecules at interfaces. *Int. J. Mod. Phys. B.* 19:691–713.
28. Shen, Y. R. 1989. Surface-properties probed by 2nd-harmonic and sum-frequency generation. *Nature.* 337:519–525.
29. Dempsey, C. E. 1990. The actions of melittin on membranes. *Biochim. Biophys. Acta.* 1031:143–161.
30. Fletcher, J. E., and M. S. Jiang. 1993. Possible mechanisms of action of cobra snake venom cardiotoxins and bee venom melittin. *Toxicon.* 31: 669–695.
31. Bechinger, B. 1997. Structure and functions of channel-forming peptides: magainins, cecropins, melittin and alamethicin. *J. Membr. Biol.* 156: 197–211.
32. Terwilliger, T. C., and D. Eisenberg. 1982. The structure of melittin. I. Structure determination and partial refinement. *J. Biol. Chem.* 257: 6010–6015.
33. Terwilliger, T. C., and D. Eisenberg. 1982. The structure of melittin. II. interpretation of the structure. *J. Biol. Chem.* 257:6016–6022.
34. Toraya, S., K. Nishimura, and A. Naito. 2004. Dynamic structure of vesicle-bound melittin in a variety of lipid chain lengths by solid-state NMR. *Biophys. J.* 87:3323–3335.
35. Lam, Y., S. R. Wassall, C. J. Morton, R. Smith, and F. Separovic. 2001. Solid-state NMR structure determination of melittin in a lipid environment. *Biophys. J.* 81:2752–2761.
36. Hewish, D. R., K. J. Barnham, J. A. Werkmeister, A. Kirkpatrick, N. Bartone, S. T. Liu, R. S. Norton, C. Curtain, and D. E. Rivett. 2002. Structure and activity of D-Pro14 melittin. *J. Protein Chem.* 21:243–253.
37. Kemple, M. D., P. Buckley, P. Yuan, and F. G. Prendergast. 1997. Main chain and side chain dynamics of peptides in liquid solution from ^{13}C NMR: melittin as a model peptide. *Biochemistry.* 36:1678–1688.
38. Yang, L., T. A. Harroun, T. M. Weiss, L. Ding, and H. W. Huang. 2001. Barrel-stave model or toroidal model? A case study on melittin pores. *Biophys. J.* 81:1475–1485.
39. Wang, F., and P. L. Polavarapu. 2003. Conformational analysis of melittin in solution phase: vibrational circular dichroism study. *Biopolymers.* 70: 614–619.
40. Constantinescu, I., and M. Lafleur. 2004. Influence of the lipid composition on the kinetics of concerted insertion and folding of melittin in bilayers. *Biochim. Biophys. Acta.* 1667:26–37.

41. Frey, S., and L. K. Tamm. 1991. Orientation of melittin in phospholipid bilayers. A polarized attenuated total reflection infrared study. *Biophys. J.* 60:922–930.

42. Kriech, M. A., and J. C. Conboy. 2003. Label-free chiral detection of melittin binding to a membrane. *J. Am. Chem. Soc.* 125:1148–1149.

43. Huang, H. W. 2000. Action of antimicrobial peptides: two-state model. *Biochemistry.* 39:8347–8352.

44. Shai, Y. 2002. Mode of action of membrane active antimicrobial peptides. *Biopolymers.* 66:236–248.

45. Bechinger, B. 2004. Structure and function of membrane-lytic peptides. *CRC Crit. Rev. Plant Sci.* 23:271–292.

46. Steinem, C., H. Galla, and A. Janshoff. 2000. Interaction of melittin with solid supported membranes. *Phys. Chem. Chem. Phys.* 2:4580–4585.

47. Allende, D., S. A. Simon, and T. J. McIntosh. 2005. Melittin-induced bilayer leakage depends on lipid material properties: evidence for toroidal pores. *Biophys. J.* 88:1828–1837.

48. Lambert, A. G., P. B. Davies, and D. J. Neivandt. 2005. Implementing the theory of sum frequency generation vibrational spectroscopy: a tutorial review. *Appl. Spectrosc. Rev.* 40:103–145.

49. Buck, M., and M. Himmelhaus. 2001. Vibrational spectroscopy of interfaces by infrared-visible sum frequency generation. *J. Vac. Sci. Technol. A.* 19:2717–2736.

50. Chen, Z., Y. R. Shen, and G. A. Somorjai. 2002. Studies of polymer surfaces by sum frequency generation vibrational spectroscopy. *Annu. Rev. Phys. Chem.* 53:437–465.

51. Shen, Y. R. 1984. The Principles of Nonlinear Optics. J. Wiley, New York.

52. Zhuang, X., P. B. Miranda, D. Kim, and Y. R. Shen. 1999. Mapping molecular orientation and conformation at interfaces by surface nonlinear optics. *Phys. Rev. B.* 59:12632–12640.

53. Wang, J., C. Y. Chen, S. M. Buck, and Z. Chen. 2001. Molecular chemical structure on poly(methyl methacrylate) (PMMA) surface studied by sum frequency generation (SFG) vibrational spectroscopy. *J. Phys. Chem. B.* 105:12118–12125.

54. Wang, J., Z. Paszti, M. A. Even, and Z. Chen. 2002. Measuring polymer surface ordering differences in air and water by sum frequency generation vibrational spectroscopy. *J. Am. Chem. Soc.* 124:7016–7023.

55. Hirose, C., N. Akamatsu, and K. Domen. 1992. Formulas for the analysis of surface sum-frequency generation spectrum by CH stretching modes of methyl and methylene groups. *J. Chem. Phys.* 96:997–1004.

56. Moad, A. J., and G. J. Simpson. 2004. A unified treatment of selection rules and symmetry relations for sum-frequency and second harmonic spectroscopies. *J. Phys. Chem. B.* 108:3548–3562.

57. Tamm, L. K., and H. M. Mcconnell. 1985. Supported phospholipid-bilayers. *Biophys. J.* 47:105–113.

58. Thompson, N. L., and A. G. Palmer. 1988. Model cell membranes on planar substrates. *Comm. Mol. Cell. Biophys.* 5:39–56.

59. Muller, D. J., M. Amrein, and A. Engel. 1997. Adsorption of biological molecules to a solid support for scanning probe microscopy. *J. Struct. Biol.* 119:172–188.

60. Kim, J., G. Kim, and P. S. Cremer. 2001. Investigations of water structure at the solid/liquid interface in the presence of supported lipid bilayers by vibrational sum frequency spectroscopy. *Langmuir.* 17:7255–7260.

61. Parthasarathy, R., P. A. Cripe, and J. T. Groves. 2005. Electrostatically driven spatial patterns in lipid membrane composition. *Phys. Rev. Lett.* 95:048101/1–048101/4.

62. Jung, S. Y., S. M. Lim, F. Albertorio, G. Kim, M. C. Gurau, R. D. Yang, M. A. Holden, and P. S. Cremer. 2003. The Vroman effect: a molecular level description of fibrinogen displacement. *J. Am. Chem. Soc.* 125:12782–12786.

63. Walker, R. A., J. A. Gruetzmacher, and G. L. Richmond. 1998. Phosphatidylcholine monolayer structure at a liquid-liquid interface. *J. Am. Chem. Soc.* 120:6991–7003.

64. Fattal, E., S. Nir, R. A. Parente, and F. C. Szoka. 1994. Pore-forming peptides induce rapid phospholipid flip-flop in membranes. *Biochemistry.* 33:6721–6731.

65. Beven, L., S. Castano, J. Dufourcq, A. Wieslander, and H. Wroblewski. 2003. The antibiotic activity of cationic linear amphipathic peptides: lessons from the action of leucine/lysine copolymers on bacteria of the class mollicutes. *Eur. J. Biochem.* 270:2207–2217.

66. Giacometti, A., O. Cirioni, W. Kamysz, G. D'Amato, C. Silvestri, M. S. Del Prete, J. Lukasiak, and G. Scalise. 2003. Comparative activities of cecropin A, melittin, and cecropin A-melittin peptide CA(1–7)M(2–9)NH2 against multidrug-resistant nosocomial isolates of acinetobacter baumannii. *Peptides.* 24:1315–1318.

67. Stocker, J. F., and J. R. Traynor. 1986. The action of various venoms on Escherichia coli. *J. Appl. Bacteriol.* 61:383–388.

68. Chen, C. Y., J. Wang, C. L. Loch, D. Ahn, and Z. Chen. 2004. Demonstrating the feasibility of monitoring the molecular-level structures of moving polymer/silane interfaces during silane diffusion using SFG. *J. Am. Chem. Soc.* 126:1174–1179.

69. Chen, X., H. Tang, M. A. Even, J. Wang, G. N. Tew, and Z. Chen. 2006. Observing a molecular knife at work. *J. Am. Chem. Soc.* 128: 2711–2714.

70. Chen, X., J. Wang, A. P. Boughton, C. B. Kristalyn, and Z. Chen. 2007. Multiple orientation of melittin inside a single lipid bilayer determined by combined vibrational spectroscopic studies. *J. Am. Chem. Soc.* 129:1420–1427.

71. Hristova, K., C. E. Dempsey, and S. H. White. 2001. Structure, location, and lipid perturbations of melittin at the membrane interface. *Biophys. J.* 80:801–811.

72. Jacobs, R. E., and S. H. White. 1989. The nature of the hydrophobic binding of small peptides at the bilayer interface: implications for the insertion of transbilayer helices. *Biochemistry.* 28:3421–3437.

73. Biggin, P. C., and M. S. P. Sansom. 1999. Interactions of α-helices with lipid bilayers: a review of simulation studies. *Biophys. Chem.* 76: 161–183.

74. Farsad, K., and P. De Camilli. 2003. Mechanisms of membrane deformation. *Curr. Opin. Cell Biol.* 15:372–381.

75. Chizmadzhev, Y. A. 2004. The mechanisms of lipid-protein rearrangements during viral infection. *Bioelectrochemistry.* 63:129–136.

76. Schibli, D. J., and W. Weissenhorn. 2004. Class I and class II viral fusion protein structures reveal similar principles in membrane fusion. *Mol. Membr. Biol.* 21:361–371.

77. Jahn, R., T. Lang, and T. C. Sudhof. 2003. Membrane fusion. *Cell.* 112:519–533.

78. Janmey, P. A., W. Xian, and L. A. Flanagan. 1999. Controlling cytoskeleton structure by phosphoinositide-protein interactions: phosphoinositide binding protein domains and effects of lipid packing. *Chem. Phys. Lipids.* 101:93–107.

79. Tanaka, M., and E. Sackmann. 2005. Polymer-supported membranes as models of the cell surface. *Nature.* 437:656–663.